Finite-temperature radiative corrections to Compton scattering

S. Varma
Department of Physics and Center for Particle Physics, The University of Texas at Austin, Austin, Texas 78712
(Received 24 February 1992)

We calculate the finite-temperature α^3 corrections to the differential and total Compton scattering cross sections. We find that it is necessary to include soft photon absorption and emission diagrams to cancel the infrared divergences in the cross section. The cross sections are evaluated for the case where the initial electron is at rest.

PACS number(s): 12.20.Ds

I. INTRODUCTION

There have been many calculations of finite-temperature corrections to various processes because, as experiments and observations have become better and produced more accurate results, it has become correspondingly necessary to make more and more exact calculations for these processes. In addition, theoretical investigations of the early Universe have also necessitated the calculation of finite-temperature corrections. Therefore, it is important to calculate at what temperatures T-dependent corrections become of sufficient magnitude to cause appreciable corrections to conventional zero-temperature results, and how large these corrections are. For example, some authors have calculated the finite-temperature corrections to the renormalization constants of QED [1–4], some have calculated helium abundance in the early Universe [5,6], and some have calculated the finite-temperature corrections to the anomalous magnetic moment of the electron [2,7–8].

However, there have not been many calculations of the corrections to fundamental scattering processes. Such processes are interesting, not only in themselves, but also as parts of other phenomenona. In this paper we shall calculate the T-dependent $O(\alpha^3)$ corrections for one such process, namely, Compton scattering, for which the zero-temperature corrections were calculated by Brown and Feynman [9]. The Compton scattering cross section, apart from its intrinsic interest, is useful in the calculation of several processes such as calculating stellar opacity [10], and calculating relic radiation [11].

For simplicity we shall work at temperatures $T=1/\beta \ll m_0$, where m_0 is the electron mass at zero temperature. This means that we can neglect all Fermi-Dirac factors because they will be suppressed by a factor $e^{-\beta m_0}$ as compared to the Bose-Einstein factors. Neglecting these factors leads to the results being gauge noninvariant but, as these effects are exponentially suppressed, one need not be concerned about them. Note that at these temperatures there are no finite-temperature corrections of order α^2 because the only possible corrections could come from the fermion propagators. Furthermore, we shall take the on-shell mass condition to be $p^2=m_0^2$. For the purposes of this paper, this is equivalent to $p^2=(m_0+m_T)^2$ because the error induced is higher order than α^3.

We have a choice of formalisms to work in as, at the one-loop level, the real-time and the imaginary-time formalisms are equivalent. In the imaginary time formalism the energy is treated as a discrete variable and one sums over energy and integrates over momenta without modifying the propagators. In the real time formalism energy is a continuous variable and one integrates as in zero-temperature field theory but with a modification to the propagators. We shall work in the real time formalism because the finite-temperature pieces are explicitly separated out from the zero-temperature ones. This has the added advantage that the ultraviolet divergences will be contained in the $T=0$ part of any diagram. Since the $T=0$ parts of the diagrams are already known, we need to only calculate the $T\neq 0$ parts of these diagrams and will thus not need to worry about ultraviolet divergences.

In the real time formalism, the tree-level electron propagator in momentum space is

$$S(p)=\frac{i}{\not p-m+i\epsilon}-2\pi\delta(p^2-m^2)(\not p+m)n_F(E_p)\ , \quad (1.1)$$

where

$$n_F(E_p)=\frac{1}{e^{\beta E_p}+1} \quad (1.2)$$

is the Fermi-Dirac distribution whose effects can be neglected, and $E_p=\sqrt{\mathbf{p}^2+m^2}$. We are using units of temperature where Boltzmann's constant is set equal to unity and the metric is $(+---)$. The tree-level photon propagator in the Landau gauge is

$$D_\beta^{\mu\nu}(q)=-g^{\mu\nu}\left[\frac{i}{q^2+i\epsilon}+2\pi\delta(q^2)n_B(E_q)\right]\ , \quad (1.3)$$

where

$$n_B(E_q)=\frac{1}{e^{\beta E_q}-1} \quad (1.4)$$

is the Bose-Einstein distribution and $E_q=|\mathbf{q}|$. We shall adopt this gauge for all the following calculations. The Feynman rules and diagrams here are exactly the same as in the zero-temperature case, but with the replacement of

these propagators for the zero-temperature ones. Note that the propagators explicitly split into zero-temperature and finite-temperature pieces making it easy to separate out the finite-temperature contributions. Note also that the Bose factor in Eq. (1.3) leads to extra infrared divergences. These are canceled, as usual, by the three-body diagrams but with the proviso that both emission and absorption diagrams be included. To avoid excessive tedium we shall not show intermediate results but will collect them all together at the end.

The organization of the paper is as follows. In Sec. II we describe the various corrections to the cross section. In Sec. III we calculate the finite-temperature corrections to the mass and wave-function renormalization constants. In Sec. IV we calculate the corrections due to the finite-temperature renormalization of the α^2 scattering cross section. Section V deals with the internal insertion diagrams. In Sec. VI we calculate the three-body cross section necessary to cancel the infrared divergences appearing in these corrections. We present and discuss our results in Sec. VII.

II. CORRECTIONS TO THE CROSS SECTION

There are several corrections of order α^3 that need to be considered. They are the following.

(1) Corrections to the Klein-Nishina cross section due to finite-temperature mass and wave-function renormalization. These are due to the external line insertion of the electron self-energy diagram, Fig. 1, which produces α^3 corrections to the cross-section.

(2) Internal insertion diagrams shown in Fig. 3.

(3) Inelastic, three-body (bremsstrahlung) processes. We must include these to cancel the infrared divergences occurring in the first two sets of corrections. The key point to note here is that electrons can be emitted to and absorbed from the heat bath. Thus we must include both absorption and stimulated emission diagrams, and these will successfully cancel the infrared divergences [3]. Stimulated emission modifies the density-of-final states factor [3] to

$$\frac{d^3q}{(2\pi)^3}\frac{1}{2E_q}[1+n_B(E_q)] \tag{2.1}$$

for bosons. Again, there is no need to include finite-temperature mass or wave-function renormalization effects.

III. MASS AND WAVE-FUNCTION RENORMALIZATION

Let us consider the electron self-energy, Fig. 1. We write $\Sigma=\Sigma_0+\Sigma_T$, where Σ_0 is the usual $T=0$ contribution. The expression for Σ is

$$-i\Sigma=(-ie)^2\int\frac{d^4k}{(2\pi)^4}\gamma^\mu S(p-k)\gamma^\nu D^{\mu\nu}(k)\ . \tag{3.1}$$

If we neglect the Fermi-Dirac factor, the $T\neq 0$ part of Σ is

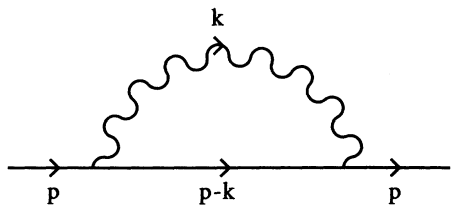

FIG. 1. The electron self-energy.

$$\Sigma_T=-\frac{2e^2}{(2\pi)^3}\int d^4k\left[\frac{2m-\not p+\not k}{(p-k)^2-m^2}n_B(k)\delta(k^2)\right]\ . \tag{3.2}$$

Since we wish to calculate the mass shift δm_β, we evaluate $\not p-m-\Sigma_T=0$ and thus must put Eq. (3.2) on shell to get

$$\Sigma_T=\frac{e^2}{(2\pi)^3}\int d^4k\,\delta(k^2)n_B(k)\frac{\not k}{p\cdot k}\equiv I \tag{3.3}$$

from which one obtains

$$I^0(p)=\frac{\pi\alpha}{6\beta^2|\mathbf{p}|}\ln\frac{p^0+|\mathbf{p}|}{p^0-|\mathbf{p}|}\ , \tag{3.4a}$$

$$I^i(p)=-\frac{\pi\alpha p^i}{3\beta^2|\mathbf{p}|^2}+\frac{\pi\alpha p^0 p^i}{6\beta^2|\mathbf{p}|^3}\ln\frac{p^0+|\mathbf{p}|}{p^0-|\mathbf{p}|}\ . \tag{3.4b}$$

Therefore,

$$m^2\equiv(p^0)^2-|\mathbf{p}|^2=m_0^2+\frac{2\pi\alpha}{3\beta^2} \tag{3.5}$$

and

$$\delta m_\beta=\frac{\pi\alpha}{3\beta^2 m_0^2}\ . \tag{3.6}$$

Note that the mass shift is independent of momentum. This is a somewhat surprising result since blackbody radiation defines a preferred frame; that it obtains is due to our neglect of the Fermi-Dirac factors in the propagators. A detailed calculation shows that momentum dependence occurs only through those terms [3].

We define the finite-temperature correction to the wave-function renormalization constant Z_2 as $\delta Z_2^T=d\Sigma_T/d\not p|_{\not p=m}$. This gives us

$$\delta Z_2^T=\frac{e^2}{2\pi}\int d^4k\,\delta(k^2)n_B(k)\frac{m^2}{(p\cdot k)^2} \tag{3.7}$$

$$=\frac{e^2}{2\pi^2}I_A\ , \tag{3.8}$$

where

$$I_A=\int_0^\infty\frac{dk}{k}n_B(k)\ . \tag{3.9}$$

IV. CORRECTIONS TO THE KLEIN-NISHINA CROSS SECTION

Figure 2 shows the Klein-Nishina diagrams. To simplify the calculation, we define the quantities

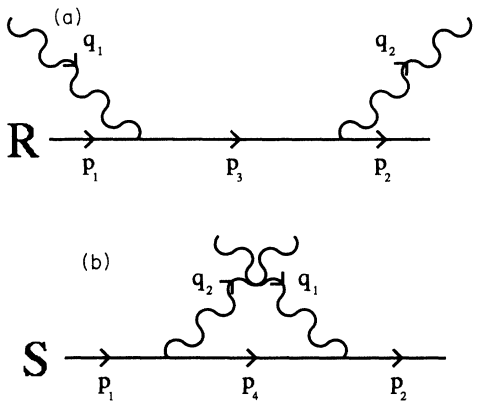

FIG. 2. The Klein-Nishina diagrams.

$$\kappa=-p_1\cdot q_1=-p_2\cdot q_2 \ , \tag{4.1}$$

$$\tau=p_1\cdot q_2=p_2\cdot q_1 \ , \tag{4.2}$$

$$\epsilon=p_1\cdot p_2 \ , \tag{4.3}$$

$$p_3=p_1+q_1=p_2+q_2 \ , \tag{4.4}$$

$$p_4=p_1-q_2=p_2-q_1 \ . \tag{4.5}$$

In terms of these quantities the matrix elements are

$$\frac{-ie^2}{2\kappa}\bar{u}(p_2)\gamma^\mu(\not{p}_3+m)\gamma^\nu u(p_1)\equiv R \ , \tag{4.6}$$

$$\frac{-ie^2}{2\tau}\bar{u}(p_2)\gamma^\nu(\not{p}_4+m)\gamma^\mu u(p_1)\equiv S \tag{4.7}$$

and, summing and averaging over polarizations and spins, we get

$$M_{\rm KN}=\tfrac{1}{4}|R+S|^2 \ . \tag{4.8}$$

The temperature corrections to $d\sigma_{\rm KN}$ are produced by a shift in the renormalization factors; i.e., we have

$$d\sigma_{\rm KN}\to d\sigma_{\rm KN}(Z_2\to Z_2^0+\delta Z_0^T, m\to m_0+\delta m_\beta) \ . \tag{4.9}$$

In the Klein-Nishina cross section we need $(Z_2)^2$. But Z_2^0 has already been taken care of by the zero-temperature renormalization so we have $(1+\delta Z_2^T)^2 \approx 1+2\delta Z_2^T$ multiplying $d\sigma_{\rm KN}$. The total correction to $d\sigma_{\rm KN}$ is then

$$d\sigma_{\rm KN}=d\sigma^0_{\rm KN}(m_0)+\frac{d[d\sigma^0_{\rm KN}(m_0)]}{dm_0}\delta m_\beta +2\delta Z_2^T d\sigma^0_{\rm KN}(m) \tag{4.10}$$

giving us two temperature corrections:

$$\frac{\pi\alpha}{3\beta^2 m_0}\frac{d[d\sigma^0_{\rm KN}(m_0)]}{dm_0} \tag{4.11}$$

and

$$\frac{e^2 I_A}{\pi^2}d\sigma^0_{\rm KN}(m) \ . \tag{4.12}$$

To this order we can put $m=m_0$ in Eq. (4.12).

V. INTERNAL INSERTION DIAGRAMS

Figure 3 shows the diagrams obtained from insertions on internal lines. To get α^3 correction, we will take the interference of these diagrams with the Klein-Nishina diagrams. However, since we are not including the modification to the electron propagator, we need only consider the interference of these diagrams with the zero-temperature Klein-Nishina diagrams. To this order, we can again put $m=m_0$ and $Z_2=Z_2^0$. The expressions for the interference of these diagrams with the Klein-Nishina diagrams are (after summing and averaging over spins and polarizations)

$$2\,{\rm Re}[J_{1,\beta}(R^*+S^*)]=\frac{-\alpha^3}{16m^2}\int d^4k\,\delta(k^2)n_B(k)\frac{1}{(p_1\cdot k)(p_2\cdot k)(p_3\cdot k+\kappa)} \times{\rm Tr}\left[(\not{p}_2+m)\gamma^\alpha(\not{p}_2-\not{k}+m)\gamma^\mu(\not{p}_3-\not{k}+m)\gamma^\nu(\not{p}_1-\not{k}+m)\gamma_\alpha(\not{p}_1+m)\times\left[\frac{1}{\kappa}\gamma_\nu(\not{p}_3+m)\gamma_\mu+\frac{1}{\tau}\gamma_\mu(\not{p}_4+m)\gamma_\nu\right]\right] , \tag{5.1a}$$

$$2\,{\rm Re}[L_{1,\beta}(R^*+S^*)]=\frac{-\alpha^3}{16m^2}\int d^4k\,\delta(k^2)n_B(k)\frac{1}{\kappa^2(p_3\cdot k+\kappa)} \times{\rm Tr}\left[(\not{p}_2+m)\gamma^\mu(\not{p}_3+m)\gamma^\alpha(\not{p}_3-\not{k}+m)\gamma_\alpha(\not{p}_3+m)\gamma^\nu(\not{p}_1+m)\times\left[\frac{1}{\kappa}\gamma_\nu(\not{p}_3+m)\gamma_\mu+\frac{1}{\tau}\gamma_\mu(\not{p}_4+m)\gamma_\nu\right]\right] , \tag{5.1b}$$

$$2\,\mathrm{Re}[K'_{1,\beta}(R^*+S^*)]=\frac{-\alpha^3}{16m^2}\int d^4k\,\delta(k^2)n_B(k)\frac{1}{\kappa(p_1\cdot k)(p_3\cdot k+\kappa)}$$
$$\times\mathrm{Tr}\left[(\not p_2+m)\gamma^\mu(\not p_3+m)\gamma^\alpha(\not p_3-\not k+m)\gamma^\nu(\not p_1-\not k+m)\gamma_\alpha(\not p_1+m)\right.$$
$$\left.\times\left[\frac{1}{\kappa}\gamma_\nu(\not p_3+m)\gamma_\mu+\frac{1}{\tau}\gamma_\mu(\not p_4+m)\gamma_\nu\right]\right], \tag{5.1c}$$

$$2\,\mathrm{Re}[K''_{1,\beta}(R^*+S^*)]=\frac{-\alpha^3}{16m^2}\int d^4k\,\delta(k^2)n_B(k)\frac{1}{\kappa(p_2\cdot k)(p_3\cdot k+\kappa)}$$
$$\times\mathrm{Tr}\left[(\not p_2+m)\gamma^\alpha(\not p_2-\not k+m)\gamma^\mu(\not p_3-\not k+m)\gamma_\alpha(\not p_3+m)\gamma^\nu(\not p_1+m)\right.$$
$$\left.\times\left[\frac{1}{\kappa}\gamma_\nu(\not p_3+m)\gamma_\mu+\frac{1}{\tau}\gamma_\mu(\not p_4+m)\gamma_\nu\right]\right]. \tag{5.1d}$$

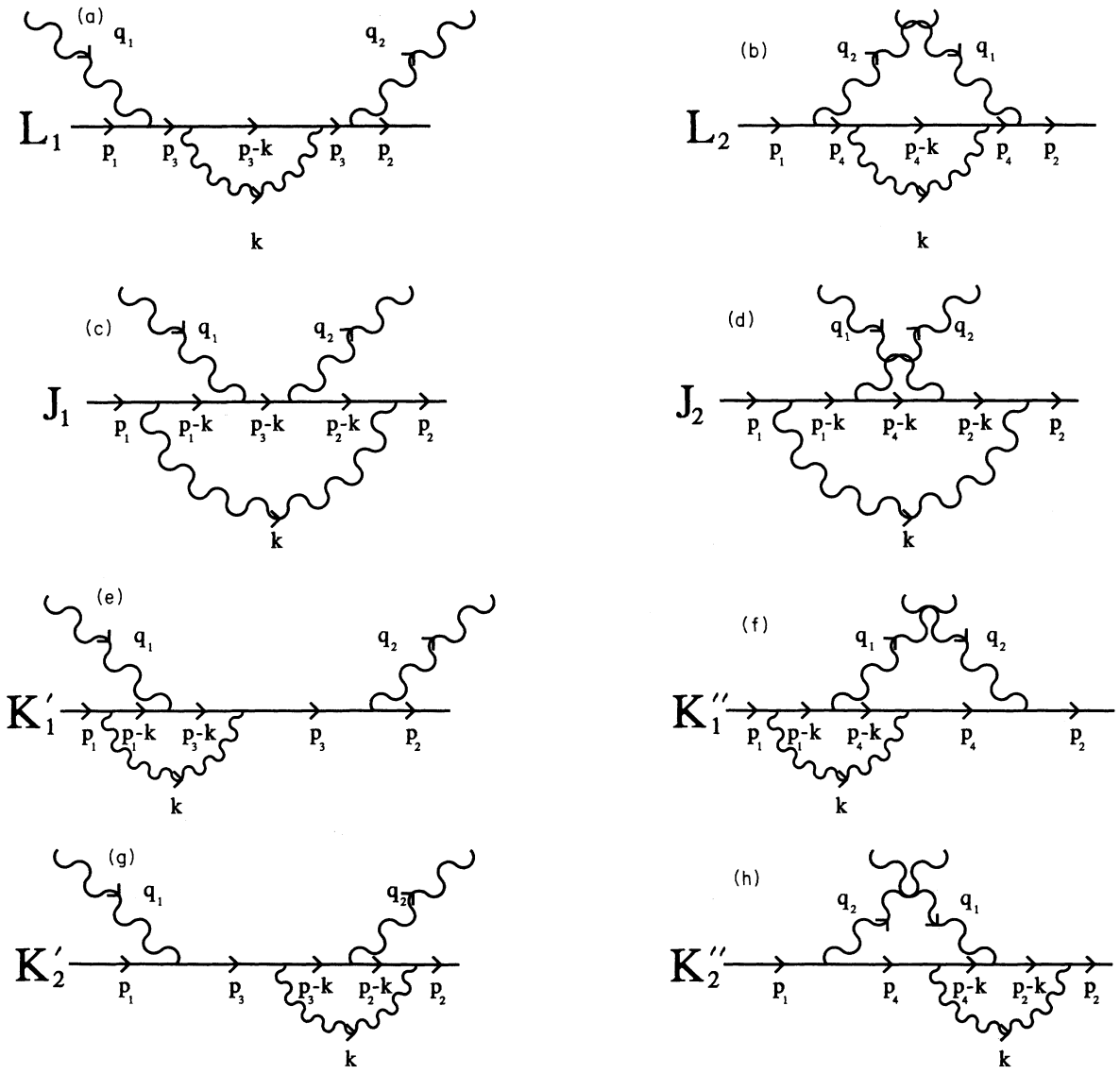

FIG. 3. The internal insertion diagrams.

We now let $p_3 \leftrightarrow p_4$ and $\kappa \leftrightarrow \tau$ in Eqs. (5.1) to account for the flipped diagrams in which emission takes place before absorption. The total contribution is then the sum of all these diagrams. In practice, one can just evaluate Eqs. (5.1) and do the substitutions at the end.

To evaluate the integrals, we expand for large κ and τ in the following manner:

$$\frac{1}{p_3\cdot k+\kappa} \approx \frac{1}{\kappa} - \frac{p_3\cdot k}{\kappa^2} , \tag{5.2}$$

$$\frac{1}{p_4\cdot k+\tau} \approx \frac{1}{\tau} - \frac{p_4\cdot k}{\tau^2} \tag{5.3}$$

and also go into the rest frame of the electron where $p_1^0 = m$ and $\mathbf{p}_1 = 0$.

Let us investigate the range of validity of the approximations (5.2) and (5.3). First, we define the dimensionless variables $k_0 = |\mathbf{k}|/m_0, \omega_0 = \omega/m_0$, and $\omega_0' = \omega'/m_0$, where ω and ω' denote the incoming and outgoing photon momenta, respectively. We shall assume that ω_0 is large and choose it to be $\omega_0 \geq 100$. We wish to find the maximum value of the variable k_0 such that the approximation is still valid. Writing $p_3\cdot k$ as $p_1\cdot k + q_1\cdot k$, integrating out the δ function, changing to dimensionless variables, and applying the conservation of four-momentum we get

$$k_0 \ll \left| \frac{\omega_0}{1 \pm \omega_0 - \omega_0 \cos[\theta]} \right| \tag{5.4}$$

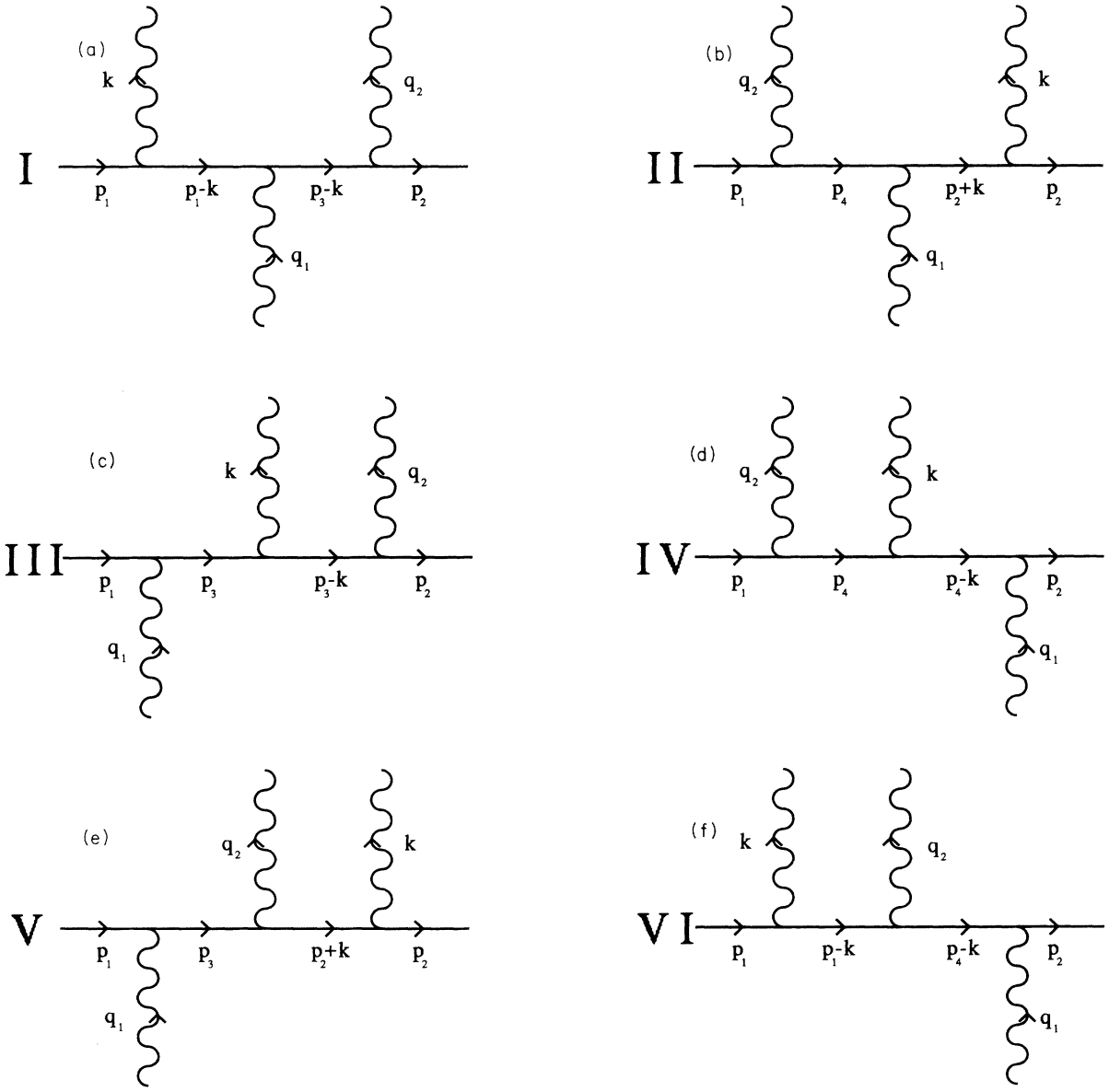

FIG. 4. The inelastic diagrams.

and similarly, writing $p_4\cdot k$ as $p_1\cdot k - q_2\cdot k$ we can derive

$$k_0 \ll \left| \frac{\omega_0'}{1 \mp \omega_0' + \omega_0' \cos[\theta]} \right| , \tag{5.5}$$

where θ is the scattering angle. For the worst case of (5.2) we find from Eq. (5.4) that $k_0 \ll 0.495$ for $\omega_0 = 100$. The worst case scenario for (5.3) for ω_0 large is different. This is because we have the relation $\omega' = m_0\omega / \{m_0 + \omega(1 - \cos[\theta])\}$. Putting this relation into Eq. (5.5) and using the worst case scenario we find that, for the approximation to be valid, we must have $k_0 \ll 0.254$. Thus, in general, this condition must be satisfied for the approximations (5.2) and (5.3) to be valid together. However, as long as the temperature $T \ll m_0$ then, as soon as k_0 attains any appreciable value, the integral will become exponentially suppressed. Therefore, if we restrict ourselves to temperatures $T \ll O(m_0)$, any values of k_0 above or close to 0.254 will be inconsequential, and the approximations (5.2) and (5.3) will be valid over all angles θ and for all values of $\omega_0 \geq 100$.

VI. INELASTIC DIAGRAMS

Figure 4 shows the inelastic scattering diagrams. Let us consider these terms for small k. In this case, the only contributions are from the terms I, II, V, and VI because the terms III and IV are negligible. Thus, with k small, we get

$$(\mathrm{I}) = \frac{e p_1^\alpha}{p_1\cdot k}\epsilon_\alpha(k) R , \tag{6.1a}$$

$$(\mathrm{II}) = \frac{e p_1^\alpha}{p_1\cdot k}\epsilon_\alpha(k) S , \tag{6.1b}$$

$$(\mathrm{V}) = \frac{-e p_2^\alpha}{p_2\cdot k}\epsilon_\alpha(k) R , \tag{6.1c}$$

$$(\mathrm{VI}) = \frac{-e p_2^\alpha}{p_2\cdot k}\epsilon_\alpha(k) S . \tag{6.1d}$$

For these diagrams, we calculate the square of the matrix element and sum over spins and polarizations. Then we let $k \rightarrow -k$ to account for the spontaneous emission process and add this back to the original matrix element. Finally we integrate the resulting expression over the finite-temperature phase space,

$$\int_0^{E_{\min}} \frac{d^3k}{(2\pi)^3}\frac{1}{2k}[1 + n_B(k)] ,$$

where $E_{\min}$ is the energy resolution of the experiment. We choose $E_{\min} \ll m_0$ and thus, as it is much smaller than all the other momenta in the problem, we neglect its effect on the momentum balance; i.e., we assume that the soft photon is emitted independent of q_2. The result for the three-body contribution then becomes

$$\frac{1}{(2\pi)^3}\int_0^{E_{\min}} \frac{d^3k}{2k}\frac{-2e^2}{4}|R+S|^2 \left[\frac{p_1^\alpha}{p_1\cdot k} - \frac{p_2^\alpha}{p_2\cdot k}\right]^2 \times[1 + n_B(k)] \tag{6.2}$$

which exactly cancels all the infrared divergences and leaves us with finite integrals.

VII. RESULTS

It is important to note that we have only calculated the finite-temperature corrections to Compton scattering to order α^3. These corrections tend to reduce both the differential and total cross sections. But, as the temperature goes up, the α^4 terms become more and more important and, at a certain point, will start to increase the cross section again. If one was to forget about these terms entirely, one would find that the cross section would seemingly become negative at higher temperatures because the finite-temperature α^3 terms would completely overwhelm the zero-temperature terms. Therefore, we have cut off our calculations when the α^3 terms reach 20% of the Klein-Nishina terms. At this point the α^4 terms are still quite small being a few percent of the Klein-Nishina terms.

The explicit expression for the correction to the differential cross section is given in the Appendix. Here we plot it for interesting values of the temperature T, momentum cutoff $E_{\min}$, and incoming photon energy ω. We also calculate the correction to the total cross section by numerically integrating the correction to the differential cross section. This is plotted in the same way as above. However, the expression has the usual forward scattering divergence. Therefore, we exclude a cone of angle 0.01 radians in the forward direction.

In each plot the corrections are expressed as a fraction of the zero-temperature Klein-Nishina results. The temperatures may be expressed in terms of degrees kelvin using the relation $m_0 = 5.93 \times 10^9$ K.

Figures 5 and 6 show the corrections to the differential cross section versus the cosine of the scattering angle at temperatures $T = 10^{-3} m_0$ and $T = 10^{-4} m_0$, respectively, for various values of ω. As ω increases, we get a larger

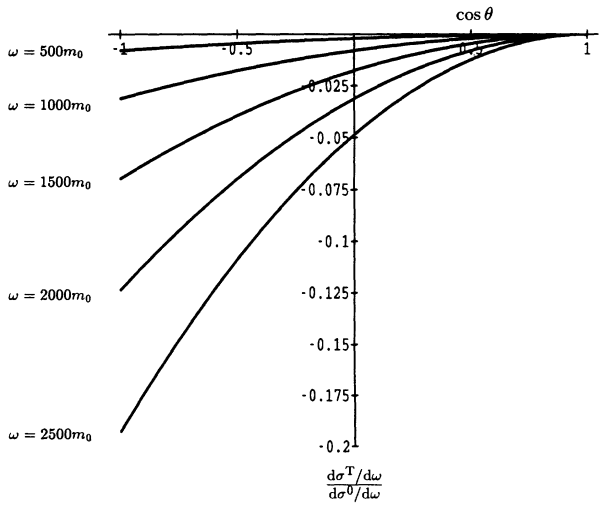

FIG. 5. Corrections to the differential cross section for $T = 10^{-3} m_0$, $E_{\min} = 10^{-2} m_0$.

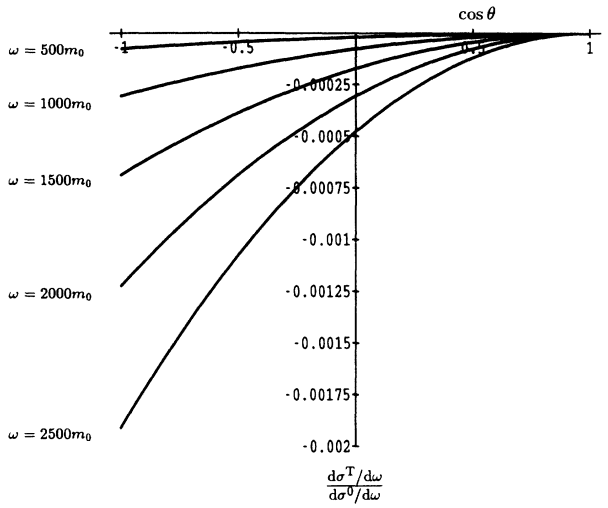

FIG. 6. Corrections to the differential cross section for $T=10^{-4}m_0$, $E_{\min}=10^{-2}m_0$.

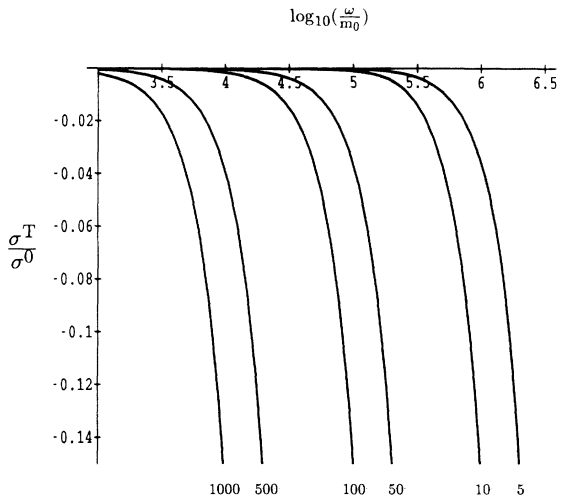

FIG. 8. Corrections to the total cross section for $E_{\min}/T=10$ for various temperatures $T(10^{-5}m_0)$, as a function of the incoming photon energy, ω.

and larger correction reaching about 19% for $\omega=2500m_0$ at $T=10^{-3}m_0$. We also clearly see that the corrections go as T^2. Further, it is interesting that the corrections become more and more important as one goes to backscattering.

Figures 7–9 show the corrections to the total cross section versus $\log_{10}(\omega/m_0)$ at various temperatures with different ways of choosing $E_{\min}$. Figure 7 shows the case where $E_{\min}=10^{-2}m_0$; i.e., the momentum cutoff is fixed independent of the temperature or the incoming momentum. Figure 8 shows the case where $E_{\min}/T=10$; i.e., the momentum cutoff is temperature dependent and is some fraction of the thermal energy. Figure 9 shows the case where $E_{\min}=10^{-10}\omega$; i.e., the momentum cutoff is some fraction of the incoming photon energy. These figures show a strong dependence on the choice of the method for calculating the momentum cutoff $E_{\min}$. For example, if we look at $\omega\approx 10^5 m_0$ then we find that a 15% correction comes about for temperatures of approximately $10^{-3}m_0$, $10^{-3}m_0$, and $10^{-6}m_0$ for Figs. 7–9, respectively. In addition, the curves for Figs. 7 and 8 show a much smaller variation with temperature than those for Fig. 9.

ACKNOWLEDGMENTS

The author would like to thank Alexander Hsieh and Eran Yehudai for their Mathematica Package, HIP [12], and Eric Myers for many useful discussions. The author has also benefited from much constructive criticism and many good suggestions from E. C. G. Sudarshan.

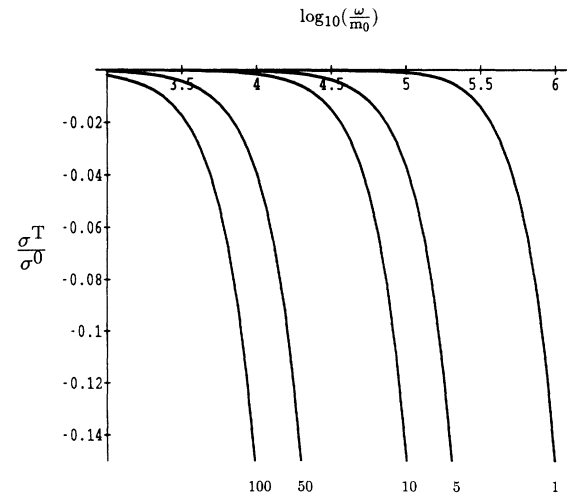

FIG. 7. Corrections to the total cross section for $E_{\min}=10^{-2}m_0$ for various temperatures $T(10^{-4}m_0)$, as a function of the incoming photon energy, ω.

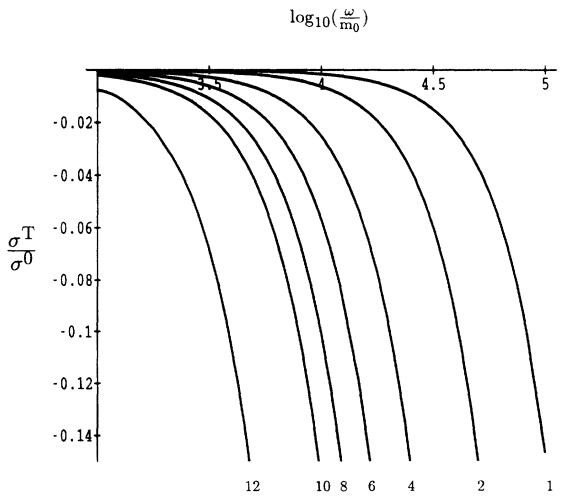

FIG. 9. Corrections to the total cross section for $E_{\min}=10^{-10}\omega$ for various temperatures $T(10^{-6}m_0)$, as a function of the incoming photon energy, ω.

APPENDIX

The explicit expression for the differential cross section is

$$\alpha^3[-4a_0i_0-8a_1i_1+2a_2(i_2+i_3)+2a_3(i_4+i_5)-4a_4(i_6+i_7)-4a_5(i_8+i_9)-4a_6(i_{10}+i_{11})+2a_7(i_{12}+i_{13})+4a_8i_{14}$$
$$+4a_9i_{15}-4a_{10}i_{16}+8a_{11}i_{17}+4a_{12}(i_{18}+i_{19})-4a_{13}(i_{20}+i_{21})+4a_{14}i_{22}+4a_{15}i_{23}-4a_{16}(i_{24}+i_{25})-4a_{17}(i_{26}+i_{27})],$$

where

$$a_0=\frac{3\epsilon}{\kappa^3}-\frac{2\epsilon}{\kappa^2m_0^2}+\frac{2}{\kappa m_0^2}-\frac{7m_0^2}{\kappa^3}+\frac{2m_0^4}{\kappa^4}+\frac{2m_0^4}{\tau^4}+\frac{3\epsilon}{\tau^3}+\frac{2\epsilon^2}{\kappa\tau^3}-\frac{7m_0^2}{\tau^3}-\frac{4\epsilon m_0^2}{\kappa\tau^3}+\frac{4m_0^4}{\kappa\tau^3}+\frac{3\epsilon}{\kappa\tau^2}$$
$$-\frac{2\epsilon}{m_0^2\tau^2}-\frac{3m_0^2}{\kappa\tau^2}+\frac{2\epsilon^2}{\kappa^3\tau}+\frac{3\epsilon}{\kappa^2\tau}-\frac{2}{\kappa\tau}+\frac{2}{m_0^2\tau}-\frac{4\epsilon m_0^2}{\kappa^3\tau}-\frac{3m_0^2}{\kappa^2\tau}+\frac{4m_0^4}{\kappa^3\tau},$$

$$a_1=\frac{-5\epsilon}{\kappa}+\frac{2\epsilon}{m_0^2}+\frac{3\epsilon^2}{\kappa m_0^2}+\frac{\epsilon m_0^2}{\kappa^2}+\frac{\epsilon m_0^2}{\tau^2}-\frac{5\epsilon}{\tau}-\frac{4\epsilon^2}{\kappa\tau}+\frac{3\epsilon^2}{m_0^2\tau}+\frac{2\epsilon^3}{\kappa m_0^2\tau}+\frac{4\epsilon m_0^2}{\kappa\tau},$$

$$a_2=\frac{2}{\kappa^2}-\frac{4}{\kappa m_0^2}+\frac{2}{\tau^2}+\frac{3\epsilon}{\kappa\tau^2}-\frac{m_0^2}{\kappa\tau^2}+\frac{3\epsilon}{\kappa^2\tau}+\frac{6}{\kappa\tau}-\frac{4}{m_0^2\tau}-\frac{4\epsilon}{\kappa m_0^2\tau}-\frac{m_0^2}{\kappa^2\tau},$$

$$a_3=\frac{6\epsilon}{\kappa^3}+\frac{12}{\kappa^2}-\frac{8\epsilon}{\kappa^2m_0^2}-\frac{2}{\kappa m_0^2}-\frac{14m_0^2}{\kappa^3}+\frac{4m_0^4}{\kappa^4}-\frac{3\epsilon}{\kappa\tau^2}+\frac{5m_0^2}{\kappa\tau^2}+\frac{4\epsilon^2}{\kappa^3\tau}+\frac{15\epsilon}{\kappa^2\tau}+\frac{2}{\kappa\tau}$$
$$-\frac{6\epsilon^2}{\kappa^2m_0^2\tau}-\frac{2\epsilon}{\kappa m_0^2\tau}-\frac{8\epsilon m_0^2}{\kappa^3\tau}-\frac{15m_0^2}{\kappa^2\tau}+\frac{8m_0^4}{\kappa^3\tau},$$

$$a_4=\frac{1}{\kappa^4}-\frac{1}{\kappa^3m_0^2},\quad a_5=\frac{1}{\kappa^3m_0^2},\quad a_6=\frac{1}{\tau^4}-\frac{1}{m_0^2\tau^3},$$

$$a_7=\frac{4m_0^4}{\tau^4}+\frac{6\epsilon}{\tau^3}+\frac{4\epsilon^2}{\kappa\tau^3}-\frac{14m_0^2}{\tau^3}-\frac{8\epsilon m_0^2}{\kappa\tau^3}+\frac{8m_0^4}{\kappa\tau^3}+\frac{12}{\tau^2}+\frac{15\epsilon}{\kappa\tau^2}-\frac{8\epsilon}{m_0^2\tau^2}-\frac{6\epsilon^2}{\kappa m_0^2\tau^2}$$
$$-\frac{15m_0^2}{\kappa\tau^2}-\frac{3\epsilon}{\kappa^2\tau}+\frac{2}{\kappa\tau}-\frac{2}{m_0^2\tau}-\frac{2\epsilon}{\kappa m_0^2\tau}+\frac{5m_0^2}{\kappa^2\tau},$$

$$a_8=\frac{-7}{\kappa^4}+\frac{3\epsilon}{\kappa^4m_0^2}+\frac{2}{\kappa^3m_0^2}+\frac{2m_0^2}{\kappa^5}-\frac{4\epsilon}{\kappa^4\tau}-\frac{3}{\kappa^3\tau}+\frac{2\epsilon^2}{\kappa^4m_0^2\tau}+\frac{2\epsilon}{\kappa^3m_0^2\tau}+\frac{4m_0^2}{\kappa^4\tau},$$

$$a_9=\frac{-2\epsilon}{\kappa^3}-\frac{1}{\kappa^2}+\frac{\epsilon^2}{\kappa^3m_0^2}+\frac{\epsilon}{\kappa^2m_0^2}-\frac{\epsilon}{\kappa^2\tau}+\frac{2m_0^2}{\kappa^2\tau},\quad a_{10}=\frac{-1}{\kappa\tau^3}+\frac{2\epsilon}{\kappa m_0^2\tau^3}-\frac{1}{\kappa^3\tau}+\frac{2\epsilon}{\kappa^3m_0^2\tau},$$

$$a_{11}=\frac{-\epsilon}{\kappa\tau^2}+\frac{\epsilon^2}{\kappa m_0^2\tau^2}-\frac{m_0^2}{\kappa\tau^2}-\frac{\epsilon}{\kappa^2\tau}+\frac{2}{\kappa\tau}+\frac{\epsilon^2}{\kappa^2m_0^2\tau}-\frac{m_0^2}{\kappa^2\tau},\quad a_{12}=\frac{1}{\kappa m_0^2\tau^2}+\frac{1}{\kappa^2m_0^2\tau},\quad a_{13}=\frac{1}{\kappa^3\tau},$$

$$a_{14}=\frac{2m_0^2}{\tau^5}-\frac{7}{\tau^4}-\frac{4\epsilon}{\kappa\tau^4}+\frac{3\epsilon}{m_0^2\tau^4}+\frac{2\epsilon^2}{\kappa m_0^2\tau^4}+\frac{4m_0^2}{\kappa\tau^4}-\frac{3}{\kappa\tau^3}+\frac{2}{m_0^2\tau^3}+\frac{2\epsilon}{\kappa m_0^2\tau^3},$$

$$a_{15}=\frac{-2\epsilon}{\tau^3}+\frac{\epsilon^2}{m_0^2\tau^3}-\frac{1}{\tau^2}-\frac{\epsilon}{\kappa\tau^2}+\frac{\epsilon}{m_0^2\tau^2}+\frac{2m_0^2}{\kappa\tau^2},\quad a_{16}=\frac{1}{m_0^2\tau^3},\quad a_{17}=\frac{1}{\kappa\tau^3},$$

$$i_0=\frac{2\pi^3}{3\beta^2},\quad i_1=\frac{2\pi F_1I_1}{m_0|\mathbf{p}_2|},\quad i_2=\frac{m_0\pi^3F_1}{3\beta^2|\mathbf{p}_2|},\quad i_3=\frac{2\pi^3p_2^0}{3\beta^2m_0},\quad i_4=\frac{2\pi^3}{3\beta^2}+\frac{2\pi^3q_1^0}{3\beta^2m_0},$$

$$i_5=\frac{2\pi^3}{3\beta^2}+\frac{\pi^3q_2^0F_1}{3\beta^2|\mathbf{p}_2|}-\frac{\pi^3\mathbf{p}_2\cdot\mathbf{q}_2}{3\beta^2|\mathbf{p}_2|^2}\left[-2+\frac{p_2^0F_1}{|\mathbf{p}_2|}\right],\quad i_6=\frac{4\pi^5m_0(m_0+q_1^0)}{15\beta^4},$$

$$i_7=\frac{4\pi^4p_2^0m_0}{15\beta^4}+\frac{4\pi^5p_2^0q_1^0}{15\beta^4}+\frac{4\pi^5\mathbf{p}_2\cdot\mathbf{q}_1}{45\beta^4},\quad i_8=\left[\frac{2m_0^2\pi^2}{5\beta^2}\right]i_{15},$$

$$i_9=\frac{4\pi^5p_2^0(m_0+q_1^0)^2}{15\beta^4m_0}+\frac{4\pi^4p_2^0|\mathbf{q}_1|^2}{45\beta^4m_0}+\frac{8\pi^5(m_0+q_1^0)\mathbf{p}_2\cdot\mathbf{q}_1}{45\beta^4m_0},\quad i_{10}=i_6(q_1^0\leftrightarrow-q_2^0,\mathbf{q}_1\leftrightarrow-\mathbf{q}_2),$$

$$i_{11}=i_7(q_1^0\leftrightarrow -q_2^0,\mathbf{q}_1\leftrightarrow -\mathbf{q}_2),\quad i_{12}=\frac{2\pi^3}{3\beta^2}-\frac{2\pi^3 q_2^0}{3\beta^2 m_0},$$

$$i_{13}=i_5(q_1^0\leftrightarrow -q_2^0,\mathbf{q}_1\leftrightarrow -\mathbf{q}_2),\quad i_{14}=\frac{4\pi^5}{15\beta^4}(m_0+q_1^0)^2+\frac{4\pi^5}{45\beta^4}|\mathbf{q}_1|^2,$$

$$\begin{aligned}i_{15}=&\frac{\pi^3(m_0+q_1^0)^2F_1}{3\beta^2|\mathbf{p}_2|m_0}+\left[\frac{4\pi^3(m_0+q_1^0)}{3\beta^2 m_0|\mathbf{p}_2|^2}-\frac{2\pi^3(m_0+q_1^0)p_2^0F_1}{3\beta^2|\mathbf{p}_2|^3 m_0}\right]\mathbf{p}_2\cdot\mathbf{q}_1\\&+2\frac{|\mathbf{q}_1|^2}{3}\left[\frac{\pi^3F_1}{6\beta^2|\mathbf{p}_2|m_0}+\frac{\pi^3p_2^0}{2\beta^2|\mathbf{p}_2|^2m_0}-\frac{\pi^3(p_2^0)^2F_1}{4\beta^2|\mathbf{p}_2|^3m_0}+\frac{\pi^3F_1}{12\beta^2|\mathbf{p}_2|m_0}\right]\\&+2(\mathbf{p}_2\cdot\mathbf{q}_1)^2\left[\frac{-\pi^3p_2^0}{2\beta^2|\mathbf{p}_2|^4m_0}+\frac{\pi^3(p_2^0)^2F_1}{4\beta^2|\mathbf{p}_2|^5m_0}-\frac{\pi^3F_1}{12\beta^2|\mathbf{p}_2|^3m_0}\right],\end{aligned}$$

$$i_{16}=\frac{4\pi^5p_2^0m_0}{15\beta^4}+\frac{4\pi^5p_2^0q_1^0}{15\beta^4}+\frac{4\pi^5\mathbf{p}_2\cdot\mathbf{q}_1}{45\beta^4}-\frac{4\pi^4q_1^0m_0}{15\beta^4}-\frac{4\pi^4(q_1^0)^2}{15\beta^4}-\frac{4\pi^5|\mathbf{q}_1|^2}{45\beta^4},$$

$$i_{17}=\frac{2\pi^3}{3\beta^3}+\frac{m_0\pi^3F_1}{3\beta^2|\mathbf{p}_2|}+\frac{2\pi^3p_2^0}{3\beta^2m_0}-\frac{1}{2}i_{15}-\frac{1}{2}i_{15}(q_1^0\leftrightarrow -q_2^0,\mathbf{q}_1\leftrightarrow -\mathbf{q}_2),\quad i_{18}=\left[\frac{2m_0^2\pi^2}{5\beta^2}\right]i_{17},$$

$$\begin{aligned}i_{19}=&\frac{4\pi^5(p_2^0)^2}{15\beta^4}+\frac{4\pi^4|\mathbf{p}_2|^2}{45\beta^4}-\frac{4\pi^5p_2^0q_1^0}{15\beta^4}-\frac{4\pi^5\mathbf{p}_2\cdot\mathbf{q}_1}{45\beta^4}-\frac{4\pi^5p_2^0(q_1^0)^2}{15\beta^4m_0}-\frac{4\pi^5p_2^0|\mathbf{q}_1|^2}{45\beta^4m_0}\\&-\frac{8\pi^5q_1^0\mathbf{p}_2\cdot\mathbf{q}_1}{45\beta^4m_0}+\frac{4\pi^5q_1^0(p_2^0)^2}{15\beta^4m_0}+\frac{4\pi^5q_1^0|\mathbf{p}_2|^2}{45\beta^4m_0}+\frac{8\pi^5p_2^0\mathbf{p}_2\cdot\mathbf{q}_1}{45\beta^4m_0},\end{aligned}$$

$$i_{20}=i_{14}-\frac{4\pi^5q_2^0(m_0+q_1^0)^2}{15\beta^4m_0}-\frac{4\pi^5q_2^0|\mathbf{q}_1|^2}{45\beta^4m_0}-\frac{8\pi^5(m_0+q_1^0)\mathbf{q}_1\cdot\mathbf{q}_2}{45\beta^4m_0},$$

$$\begin{aligned}i_{21}=&\frac{4\pi^5m_0^2}{15\beta^4}+\frac{4\pi^5(q_1^0)^2}{15\beta^4}+\frac{4\pi^5|\mathbf{q}_1|^2}{45\beta^4}+\frac{8\pi^5m_0q_1^0}{15\beta^4}-\frac{2m_0^2\pi^2}{5\beta^2}\left[\frac{\pi^3q_1^0F_1}{3\beta^2|\mathbf{p}_2|}-\frac{\pi^3\mathbf{p}_2\cdot\mathbf{q}_1}{3\beta^2|\mathbf{p}_2|^2}\left[-2+\frac{p_2^0F_1}{|\mathbf{p}_2|}\right]\right]\\&-\frac{2\pi^5(q_1^0)^3F_1}{15\beta^4|\mathbf{p}_2|}+\frac{4\pi^5(q_1^0)^2\mathbf{p}_2\cdot\mathbf{q}_1}{5\beta^4|\mathbf{p}_2|^2}-\frac{2\pi^5(q_1^0)^2\mathbf{p}_2\cdot\mathbf{q}_1p_2^0F_1}{5\beta^4|\mathbf{p}_2|^3}\\&+3q_1^0\left[|\mathbf{q}_1|^2\left[\frac{2\pi^5F_1}{45\beta^4|\mathbf{p}_2|}+\frac{2\pi^5p_2^0}{15\beta^4|\mathbf{p}_2|^2}-\frac{\pi^5(p_2^0)^2F_1}{15\beta^4|\mathbf{p}_2|^3}+\frac{\pi^5F_1}{45\beta^4|\mathbf{p}_2|}\right]\right.\\&\left.+(\mathbf{p}_2\cdot\mathbf{q}_1)^2\left[\frac{-2\pi^5p_2^0}{5\beta^4|\mathbf{p}_2|^4}+\frac{\pi^5(p_2^0)^2F_1}{5\beta^4|\mathbf{p}_2|^5}-\frac{\pi^5F_1}{15\beta^4|\mathbf{p}_2|^3}\right]\right]\\&+\frac{6|\mathbf{q}_1|^2\mathbf{p}_2\cdot\mathbf{q}_1}{5|\mathbf{p}_2|^2}\left[\frac{2\pi^5}{15\beta^4}-\frac{\pi^5p_2^0F_1}{15\beta^4|\mathbf{p}_2|}+\frac{5}{2|\mathbf{p}_2|^2}\left[\frac{2\pi^5|\mathbf{p}_2|^2}{25\beta^4}-\frac{\pi^5p_2^0|\mathbf{p}_2|F_1}{25\beta^4}-\frac{2\pi^5(p_2^0)^2}{15\beta^4}-\frac{2\pi^5|\mathbf{p}_2|^2}{45\beta^4}+\frac{\pi^5(p_2^0)^3F_1}{15\beta^4|\mathbf{p}_2|}\right]\right]\\&-\frac{5(\mathbf{p}_2\cdot\mathbf{q}_1)^3}{|\mathbf{p}_2|^6}\left[\frac{2\pi^5|\mathbf{p}_2|^2}{25\beta^4}-\frac{\pi^5p_2^0|\mathbf{p}_2|F_1}{25\beta^4}-\frac{2\pi^5(p_2^0)^2}{15\beta^4}-\frac{2\pi^5|\mathbf{p}_2|^2}{45\beta^4}+\frac{\pi^5(p_2^0)^3F_1}{15\beta^4|\mathbf{p}_2|}\right]\\&-\frac{4\pi^5m_0(q_1^0)^2F_1}{15\beta^4|\mathbf{p}_2|}-2m_0\left[|\mathbf{q}_1|^2\left[\frac{2\pi^5F_1}{45\beta^4|\mathbf{p}_2|}+\frac{2\pi^5p_2^0}{15\beta^4|\mathbf{p}_2|^2}-\frac{\pi^5(p_2^0)^2F_1}{15\beta^4|\mathbf{p}_2|^3}+\frac{\pi^5F_1}{45\beta^4|\mathbf{p}_2|}\right]\right.\\&\left.+(\mathbf{p}_2\cdot\mathbf{q}_2)^2\left[\frac{-2\pi^5p_2^0}{5\beta^4|\mathbf{p}_2|^4}+\frac{\pi^5(p_2^0)^2F_1}{5\beta^4|\mathbf{p}_2|^5}-\frac{\pi^5F_1}{15\beta^4|\mathbf{p}_2|^3}\right]\right]\\&-\frac{16\pi^5m_0q_1^0\mathbf{p}_2\cdot\mathbf{q}_1}{15\beta^4|\mathbf{p}_2|^2}+\frac{8\pi^5m_0q_1^0\mathbf{p}_2\cdot\mathbf{q}_1p_2^0F_1}{15\beta^4|\mathbf{p}_2|^3},\end{aligned}$$

$$i_{22}=i_{14}(q_1^0\leftrightarrow -q_2^0,\mathbf{q}_1\leftrightarrow -\mathbf{q}_2),\quad i_{23}=i_{15}(q_1^0\leftrightarrow -q_2^0,\mathbf{q}_1\leftrightarrow -\mathbf{q}_2),$$

$$i_{24}=i_8(q_1^0\leftrightarrow -q_2^0,\mathbf{q}_1\leftrightarrow -\mathbf{q}_2),\quad i_{25}=i_9(q_1^0\leftrightarrow -q_2^0,\mathbf{q}_1\leftrightarrow -\mathbf{q}_2),$$

$i_{26}=i_{20}(q_1^0\leftrightarrow -q_2^0,\mathbf{q}_1\leftrightarrow -\mathbf{q}_2)$, $i_{27}=i_{21}(q_1^0\leftrightarrow -q_2^0,\mathbf{q}_1\leftrightarrow -\mathbf{q}_2)$

in which we have defined $F_1\equiv \ln[(p_2^0+|\mathbf{p}_2|)/(p_2^0-|\mathbf{p}_2|)]$ and $I\equiv\int_0^\infty (dk/k)n_B(k)$. Note that the infrared divergence in integral I_1 is canceled by Eq. (6.2).

[1] S. Glashow, E. C. G. Sudarshan, and A. Yildiz (unpublished).

[2] G. Peressutti and B.-S. Skagerstam, Phys. Lett. **110B**, 406 (1982).

[3] John F. Donoghue and Barry R. Holstein, Phys. Rev. D **28**, 340 (1983); **29**, 3004 (1984).

[4] K. Ahmed and Samina Saleem, Phys. Rev. D **35**, 1861 (1987).

[5] Jean-Luc Cambier, Joel R. Primack, and Marc Sher, Nucl. Phys. **B209**, 372 (1982).

[6] D. A. Dicus, E. W. Kolb, A. M. Gleeson, E. C. G. Sudarshan, V. L. Teplitz, and M. S. Turner, Phys. Rev. D **29**, 2694 (1982).

[7] Yasushi Fujimoto and Jae Hyung Yee, Phys. Lett. **114B**, 359 (1982).

[8] Paul H. Cox, William S. Heldman, and Asim Yildiz, Ann. Phys. (N.Y.) **154**, 211 (1984).

[9] L. M. Brown and R. P. Feynman, Phys. Rev. **85**, 231 (1952).

[10] Richard Bowers and Terry Deeming, *Astrophysics 1* (Jones and Bartlett, Boston, 1984), pp. 116 and 117.

[11] Ya. B. Zeldovich and I. D. Novikov, *The Structure and Evolution of the Universe* (The University of Chicago Press, Chicago, 1983), Vol. 2, pp. 189–233.

[12] Alexander Hsieh and Eran Yehudai, Comput. Phys. **6**, 253 (1992).